Transport optics for a space-charge broadening ion beam

Geoffrey P. Malafsky and Nicholas Winograd

The Pennsylvania State University, 152 Davey Laboratory, Department of Chemistry, University Park, Pennsylvania 16802

(Received 15 February 1988; accepted for publication 7 April 1988)

The design and performance of a low-energy ion gun system suitable for surface analysis is described. The ion gun system is capable of delivering up to a 0.72 μA beam of Ar^+ ions at a potential of 500 eV into a spot diameter of 1 mm. This performance is accomplished by using ion optics to refocus the space-charge diverging beam along the 44-cm path to the target. The ion optics have been optimized by the use of a new simulation program, CHDEN, which can model a series of lenses and the effects of space-charge forces.

INTRODUCTION

Beams of low-energy ions (< 1000 eV) are commonly used in surface studies. Surface penetration and disruption is reduced as the incident ion kinetic energy is lowered.[1] This effect has been utilized in secondary ion mass spectrometric (SIMS) investigations of metal-adsorbate systems to increase the structural information that may be deduced from the secondary ion spectra.[1–4] It has been proposed that bonding sites may be determined when low kinetic energy particles are used as the probe.[1,2] Beams with energies as low as 50 eV have been used to elucidate the mechanisms of sputtering experimentally[5,6] and theoretically.[7] In addition, SIMS depth profiling of semiconductors has been shown to be sensitive to the ion beam energy[8] as has the modification of depositing films by ion irradiation.[9]

Until now, the low-energy ion beams used for surface analysis have been of low current (< 100 nA) or large diameter (> 2 mm). A high current (~ 1 μA) and small diameter (~ 1 mm) beam would be useful for applications such as time-of-flight (TOF) SIMS and depth profiling. In TOF SIMS, each pulse of the primary beam must contain enough ions to produce a detectable secondary ion signal and be of short enough duration to allow adequate resolution in the mass spectrum. A 1-μA beam with a pulse period of 200 ns into a 1-mm-diam spot yields an ion flux of approximately 10^8 ions/cm^2 per pulse which is consistent with the ion doses used in static SIMS. The small beam diameter increases the resolution of studies which are sensitive to the surface structure, such as the measurement of the angular desorption patterns from single crystals. Also, the small beam diameter permits a higher spatial resolution during depth profiling studies. The high current is needed in depth profiling to remove the sample at a reasonable rate. High current is especially important at low primary ion energies due to the low sputter efficiency.

We will present an account of the design and performance of an ion gun system suitable for use with a surface analytical chamber which is capable of producing a focused, low-energy, high current beam. This system consists of three items: (a) a commercial ion source, (b) added transport optics, and (c) an UHV chamber containing a grounded sample and several surface-sensitive spectroscopies. The ion optics have been optimized by computer simulations to transport a beam of Ar^+ ions of 500-eV kinetic energy and a current of approximately 1 μA over a distance of 44 cm to produce a spot of diameter 1 mm. This beam has a high space-charge divergence which causes significant difficulties in its transport.

I. APPARATUS

The ion optics assembly is composed of three Einzel lenses and a set of x, y raster plates (Fig. 1). Lens 1 is located within the ion gun housing. Lenses 2 and 3 are placed in the main chamber. The x, y plates are at the exit of lens 3 and allow the ion beam to be rastered over an area of 1.5 cm^2 for sputter cleaning of the sample.

The optics assembly is constructed of UHV-compatible materials. The lens elements are made of 304 stainless steel and are supported by No. 0-80 stainless-steel threaded rod and 3.175-mm-diam (o.d.) alumina tubing. The lens supports are machined from the lens elements which avoids the problem of warpage resulting from welding support parts to the thin-walled lenses. A gate valve is installed between the ion gun and the main chamber to permit independent venting of the two chambers. This arrangement places the ion source 82 cm from the target while the Wien filter is 44 cm away.

In a typical UHV chamber equipped with surface analytical spectroscopies, the sample area is crowded with components. The components are grounded and it would be difficult to modify the instrumentation to have the sample holder and neighboring analysis equipment maintained at a floating potential. Therefore, it would be advantageous to have a primary ion beam apparatus which would operate referenced to ground potential and not interfere with the spectroscopic components near the sample. As we will explain in the next section, operating the low-energy ion beam assembly referenced to ground potential restricts our ability to control the space-charge divergence.

Our experimenta' arrangement imposes the additional constraint that the sample area be free of electric fields. The ion beam system is installed in an UHV chamber with the capability to perform angle-resolved SIMS (ARSIMS) experiments.[10] The measured secondary ion angular and energy distributions would be perturbed by the presence of an electric field in the vicinity of the sample. Therefore, the

 0034-6748/88/081294-09$01.30 © 1988 American Institute of Physics

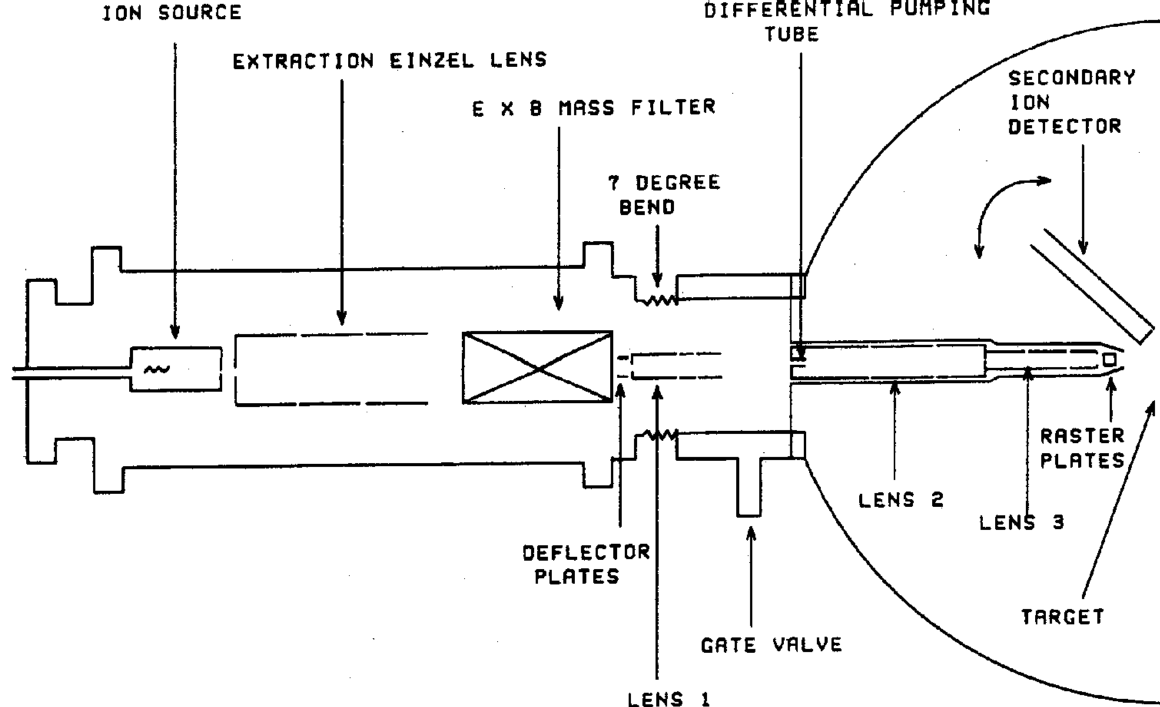

FIG. 1. Schematic diagram of the ion gun and the UHV chamber with the new ion optics.

sample is fixed at ground potential and the primary ion beam optics operated referenced to ground potential. In order to eliminate stray electric fields due to lenses 2 and 3, they are enclosed by a grounded tube.

The spacing between the sample and the grounded tube influences the detected angular desorption patterns. The secondary ion detector rotates about the sample (Fig. 1). At small angles to the axis perpendicular to the sample, the detector can collide with lenses 2 and 3. The lenses must have a small diameter to minimize this obstruction. In addition, a portion of the desorbing particles will be blocked by lens 3. We wish the separation to be small in order to reduce the drift length of the beam. The grounded tube is tapered and separated from the target by 2.5 cm as a compromise between the two competing criteria. The grounded tube has a diameter of 1.27 cm closest to the sample which blocks particles leaving the surface at angles of 17° or less.

II. BEAM TRANSPORT

The most difficult aspect of the system is the transferal of the beam from the source to the sample. The transport optics must minimize current loss due to either lens aberrations or space-charge broadening. In this section, we describe the method used to achieve this goal.

A. Space-charge divergence

A measure of the importance of coulombic repulsion within the ion beam is given by the perveance P as

$$P = IV^{-3/2}, \tag{1}$$

where I is the beam current and V its potential. As can be seen from Eq. (1), the perveance is a stronger function of the beam potential than its current. This increases the difficulty of transporting a beam at low energy and explains the popularity of various modes of decelerating the beam just prior to the target.[9,11] Some of these schemes preclude the detection of sputtered particles. For example, Thomas *et al.* placed their target within the last element of the deceleration lens.[9] A grounded sample was used with a low-energy ion beam at a few μA but this beam had a diameter of several mm.[12]

An ion beam will broaden as it travels in a manner dependent upon its perveance. The distance in which its diameter will double is estimated by[13]

$$Z/r_0 = 0.75P^{-1/2}, \tag{2}$$

where r_0 is the initial radius and P is in μperv. For a 500-eV, 1-μA, 1-mm-diam beam of Ar^+ ions, this distance is

$$Z = 4 \text{ cm}. \tag{3}$$

Partial neutralization of the beam by secondary electrons will reduce the space-charge divergence. Secondary electrons from sputtering of the lens elements will be attracted to the positively charged beam and become trapped in the potential well.[14] This will result in reduced repulsion between the positive ions. In addition, slow ions produced by charge exchange reactions between the extracted ion beam and residual gas atoms will be poorly focused by the lens and can contribute to the sputtering of the lens. The influence of the charge exchange reaction on the ion beam may be estimated by[15]

$$i_{ce}/i_B = nLQ, \tag{4}$$

where i_{ce} is the ion current due to charge exchange, i_B is the

extracted ion beam current, n is the residual gas density, L is the path length, and Q is the cross section for charge exchange. For a residual gas pressure of 5.5×10^{-6} Torr of argon and an ion beam energy of 500 eV, the values for these parameters are: $n = 1.8\times10^{11}$ atoms/cm^3, $L = 38$ cm, $Q = 2.5\times10^{-15}$ cm^2. The calculated ratio 0.017 corresponds to approximately 10^{11} ions/s produced by charge exchange reactions for a 1-μA beam.

B. Computer modeling

Extant published data on ion optics are generally limited to a few geometries and to the paraxial ray approximation.[16,17] Paraxial rays are defined to be close to the lens axis and to have a small radial velocity component.[13] Actual beams may be largely nonparaxial. The nonparaxial paths can focus at a much different point than the paraxial image plane. In Fig. 2, two rays are shown passing through a typical three-cylinder Einzel lens. The paraxial ray stays near the lens axis at all times and is focused at the image plane position of 6.3D, where D is the diameter of the lens. The other ray starts at a radial position of 0.2D and is, therefore, nonparaxial. At the paraxial image plane, this ray is greatly out of focus and at a position further off axis than predicted by the linear magnification factor calculated from paraxial theory.

We have developed a new computer program to study a variety of lens configurations and ion paths. CHDEN[18] is based on the charge-density method[16,19] and is able to trace nonparaxial as well as paraxial rays with or without the effect of space-charge divergence included. It operates on an IBM PC or compatible and calculates paths in a few minutes. The program allows the modeling of lenses with ten elements, variable diameters, variable gap widths (including zero), and with variable accuracy. A multielement lens or series of lenses separated by a gap may be modeled and the applied voltages optimized for the total ion path. A novel matrix inversion routine developed permits the simulations to run on the PC in contrast to other simulation programs requiring a mainframe computer.[16]

The charge-density method calculates the accumulated surface charge on the lens elements due to the applied voltages. The lens is divided into N subsections. The charge density across each subsection is assumed to be constant, although this is not a requirement of the technique.[19] The distribution of the subsections across the lens is a program parameter and in practice is made denser near the gap regions where the electric field gradient is highest. An $N\times N$ dense matrix relating the charge density on each subsection is generated and the following matrix equation solved to yield the charge-density distribution:

$$[\sigma] = [C]^{-1}[V], \tag{5}$$

where $[\sigma]$ is a vector matrix of the charge densities, $[C]$ is the coefficient matrix, and $[V]$ is a vector matrix of the applied voltages. Once $[\sigma]$ is known, the potential and electric field at any point in the lens space may be computed from the equations used to generate the coefficient matrix.[19] The particle path through the lens is determined by solving New-

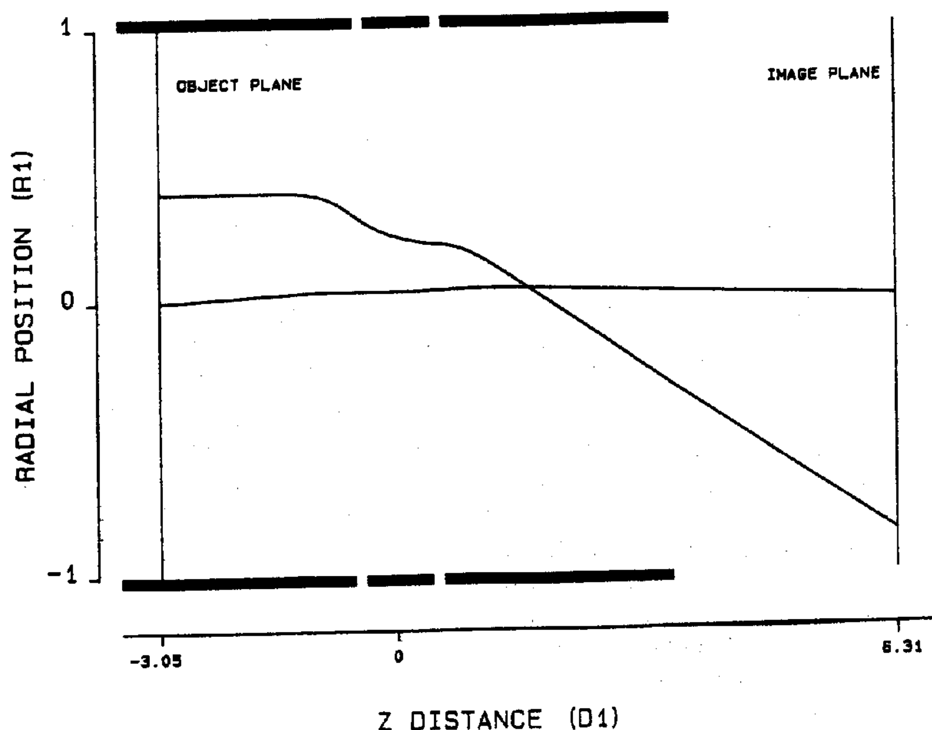

FIG. 2. Calculated ion trajectories for an Einzel lens with the central element 0.9D long. The voltage ratio V_2/V_1 is 4.1. The focal data are: object plane position (P/D) 3.05, image plane position (Q/D) 6.31, and linear magnification (M) 2.0. The ray positions at the object and image planes are (r/R, θ): ray 1: object (0,0.5°) image (0, $-$0.25°), ray 2: object (0.4,0°) image ($-$0.86, $-$5.6°). The object and image plane positions are relative to the reference plane at the geometric center of the lens.

ton's equation of motion at each subsection for the radial and axial components.

The program CHDEN incorporates the effect of space charge in a simple yet accurate manner which does not increase the computation time. The additional outward radial velocity component due to coulombic repulsion is calculated by the application of Gauss' law to the beam as it is traced through the lens. At each subsection, the additional divergence due to space charge on each particle is given by

$$E_{sc} = Itr/2\pi\epsilon R^2 w, \quad (6)$$

where E_{sc} is the radial electric field vector, I is the beam current, t is the time to cross the width w of the subsection, r is the radial position of the particle, R is the maximum radius of the beam at that subsection, and ϵ is the permittivity of vacuum. The time t is found from the axial velocity component and is dependent upon the mass of particle. This derivation assumes a constant volume density for the ion beam but other density functions may also be modeled. The space-charge electric field vector is added to the radial field vector calculated due to the action of the lens and the resultant velocity is used to compute the new radial position of the particle. This method is a first-order correction for space charge but has yielded calculated paths to within a few percent of the paths predicted by a derivation for a laminar beam of paraxial particles.[13] Other methods of space-charge inclusion have been described but are not as simple or computationally quick to implement.[19]

C. Ion source

A Colutron model 100 (Colutron Corp., Boulder, CO) ion source was chosen since it can produce ion beams of several μA at several hundred volts into the keV range.[20] The extracted ion beam has a narrower energy spread and is better collimated than a beam from a source such as the duoplasmatron. The duoplasmatron produces an intense beam but has a high angular divergence and energy spread.[21] These features cause increased loss in the transport of the beam due to geometric and chromatic aberrations in the ion optics.

In addition to the ion source, Colutron provides an Einzel lens and Wien filter with their ion gun system (model G-2). The Einzel lens serves to both extract and focus the ion beam. This lens is normally operated as a decelerating lens. However, using the lens in the accelerating mode increased the beam current transmitted through the velocity filter by about 60% at a 500-eV beam potential. This is presumably due to the reduced aberrations in the beam in the accelerating mode. The velocity filter is a 15-cm-long $E \times B$ filter (model 600-B) and is capable of mass resolution ($M/\Delta M$) of 400. It is operated in a low resolution mode.

The ion source is pumped by a 170-ℓ/s turbomolecular pump. During operation, the pressure in the source region is 2×10^{-2} Torr while the pressure in the main body of the ion gun system is 5×10^{-6} Torr.

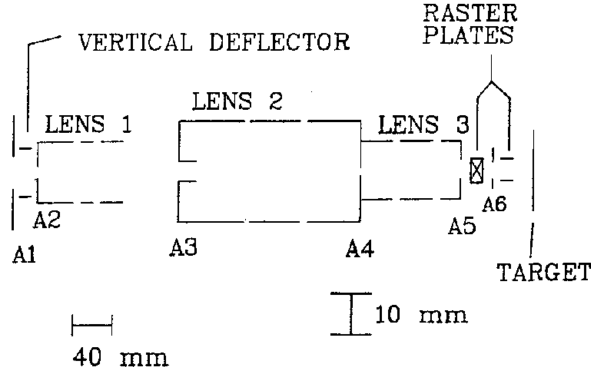

FIG. 3. Schematic diagram of the lenses and deflector plates added by the authors. Apertures A1 and A6 are grounded plates used to support the deflector plates. The dimensions are listed in Table I. The drawing is to scale.

D. Lenses

The program CHDEN was used to match the emittance of the ion beam from one lens to the acceptance of another. Although the space-charge version of CHDEN was not available during the design of the ion optics, an effort was made to design the lenses allowing for beam spreading. For all calculations, the number of sections used was 200.

The lenses are shown schematically in Fig. 3 and the dimensions listed in Table I. The lengths of the individual elements of each lens are given in units of the diameter of that lens as is the practice in charged particle optics. Each lens has three elements of cylindrical symmetry and is operated with the outer elements grounded. This prevents the creation of electric fields at the entrance and exit of the lenses due to interaction with the grounded chamber.

The important features of each lens are explained below.

1. Lens 1

This lens serves to refocus the beam as it leaves the velocity filter through the gate valve. The gate valve introduces a distance of 60 mm through which the beam must drift. At

TABLE I. Dimensions of the three Einzel lenses designed by the authors. The lens element and gap lengths are given in units of the diameter of the lens. Drift space: (1) lens 1 to lens 2: 60 mm, (2) lens 3 to target: 38 mm.

Lens No.	Diameter (mm)	Element 1	Element 2	Element 3	Gap
1	14.94	2.5D	0.9D	1.5D	0.1D
2	25.40	2.6D	2.0D	2.1D	0.1D
3	15.24	2.2D	2.0D	1.4D	0.1D

Aperture	Diameter (mm)
1	8
2	3
3	5
4	2
5	4
6	4

the entrance of this lens is a set of deflector plates which can correct for a 7° bend between the Wien filter and lens 1. This bend is intended for rejection of neutral particles but has not been used in this study. A 3-mm aperture in the first element serves to define the beam as it exits the Wien filter and to isolate stray fields due to the deflector plates.

The first element is $2.5D$ long in order to further assure the isolation of the electric field within the lens from the electric field due to the deflector plates. The field due to the gap region of the lens extends outward from the gap approximately $1.4D$.[16] Thus, the outer elements of a lens should be at least this long in order to avoid perturbations in the lens due to external fields. The last element length of $1.5D$ and the center element length of $0.9D$ were chosen so as to maximize the diameter of the lens. Generally, increasing the diameter of a lens improves its transport efficiency since more particles may follow paraxial paths.

2. Lens 2

A new geometry has been chosen for lens 2 which provides a longer focusing region than do previously published configurations.[16,17] Since the electric field extends away from the lens gap region approximately a distance of $1.4D$, a three-element lens may have its center element extended to greater than $2D$ while still maintaining an overlap of the field from each gap area. We have investigated the properties of a lens geometry with the central element $2D$ long. Figures 4 and 5 display the calculated paraxial focal data for this configuration. The object plane P and image plane Q have units of the lens diameter and are measured with respect to the reference plane which is at the geometric center of the lens. The linear magnification factor is defined as the ratio of the radial displacement at the image plane to the radial displacement at the object plane for a paraxial ray which makes an angle of 0° with the axis at the object plane. The spherical aberration coefficient C_s is given by[16]

$$C_s = \Delta r / M\alpha^3,$$

where Δr is the radial displacement at the image plane of a paraxial ray which starts at the object plane on the lens axis with an angle α, and M is the linear magnification. The lens voltages are given as the ratio of the voltage of the center element (V_2) to the voltage of the outer elements (V_1). These voltages are referenced to a zero kinetic energy particle. Figure 6 shows similar data for a lens with a central element length of $0.9D$ from Ref. 16.

A 5-mm-diam, 12.7-mm-long tube is machined into the first element of this lens to provide for differential pumping of the ion gun and main chamber. During operation, the main chamber is at a pressure of 8×10^{-9} T while the ion gun is at 5×10^{-6} T. This yields a differential pressure factor of 625.

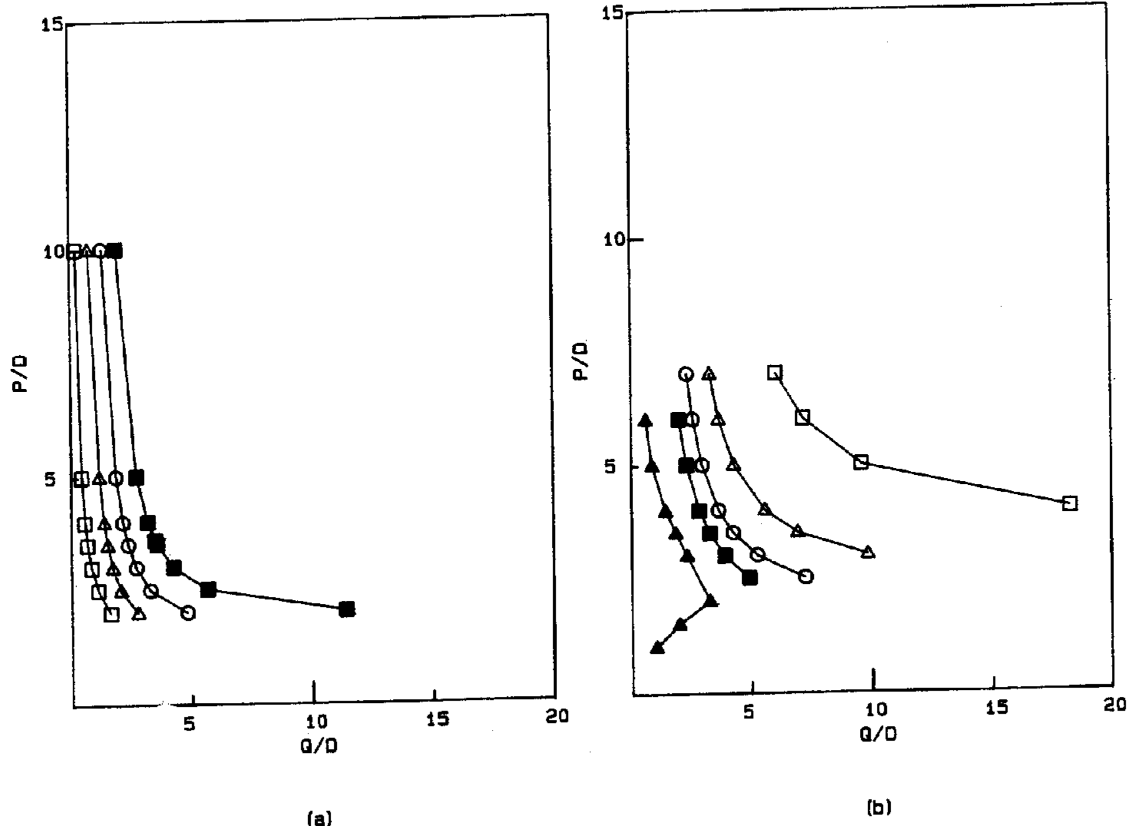

FIG. 4. The calculated focal data for the new extended Einzel lens configuration. The central element length is $2D$. Indicated are the object plane position (P/D) vs the image plane position (Q/D) for various voltage ratios. (a) □ = 0.05, △ = 10, ○ = 0.15, ■ = 0.20; (b) □ = 3, △ = 4, ○ = 5, ■ = 6, ▲ = 10.

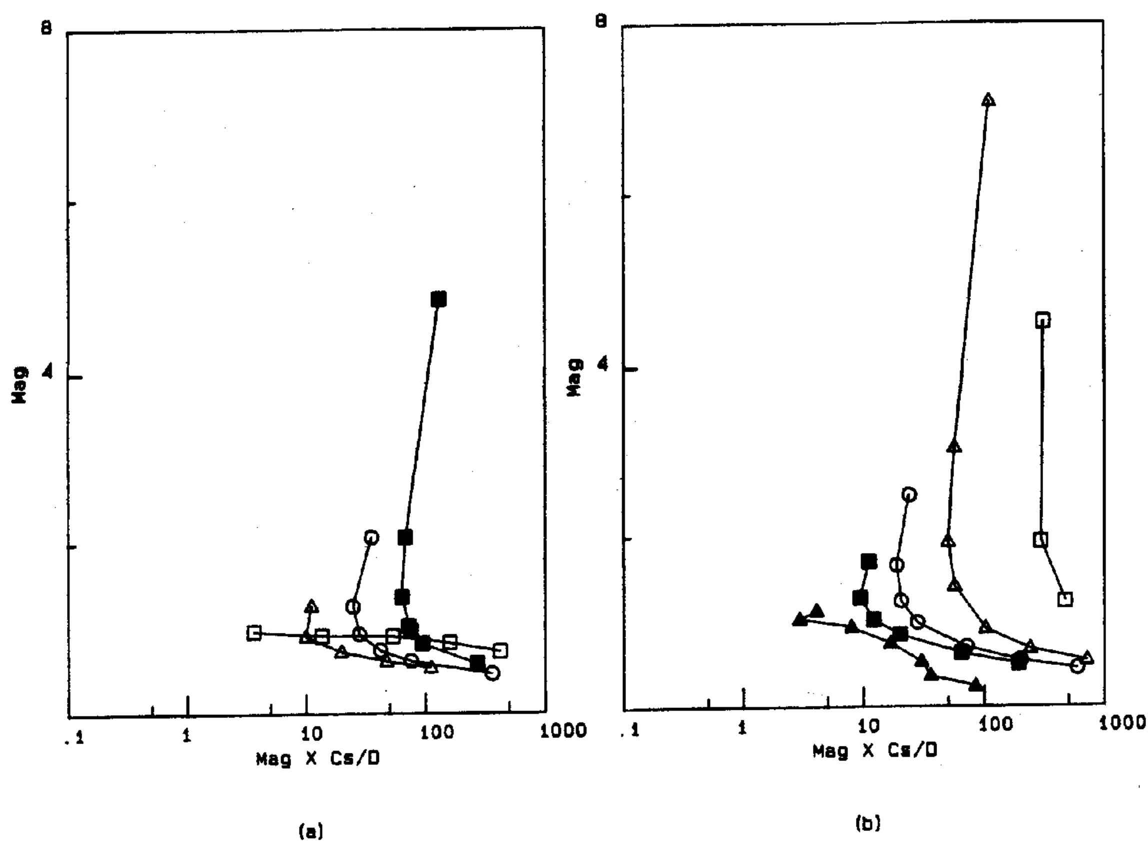

FIG. 5. The calculated focal data for the new extended Einzel lens configuration. The linear magnification factor is plotted vs the product of the magnification factor and the spherical aberration coefficient (C_s) for various voltage ratios. (a) □ = 0.05, △ = 0.10, ○ = 0.15, ■ = 0.20; (b) □ = 3, △ = 4, ○ = 5, ■ = 6, ▲ = 10.

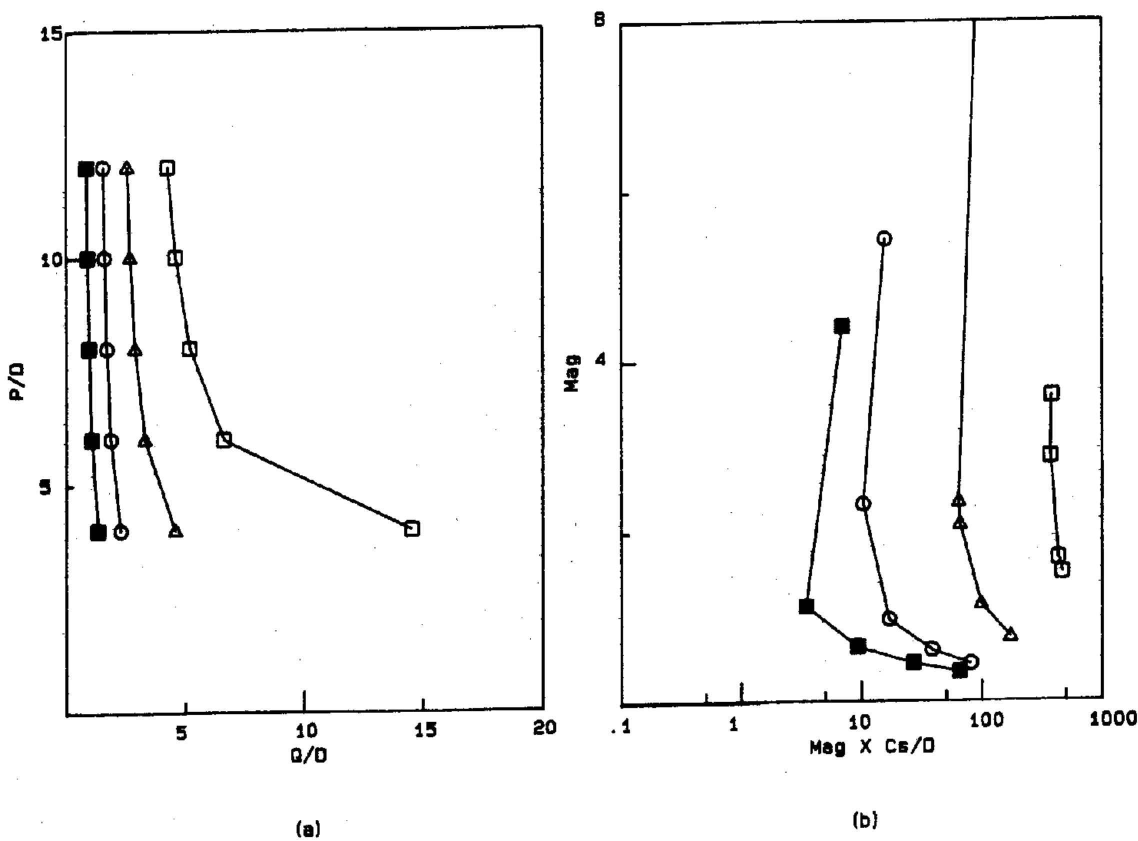

FIG. 6. Focal data from Ref. 16 for an Einzel lens with a central element length of 0.9D. Several voltage ratios are displayed. □ = 3, △ = 4, ○ = 6, ■ = 10.

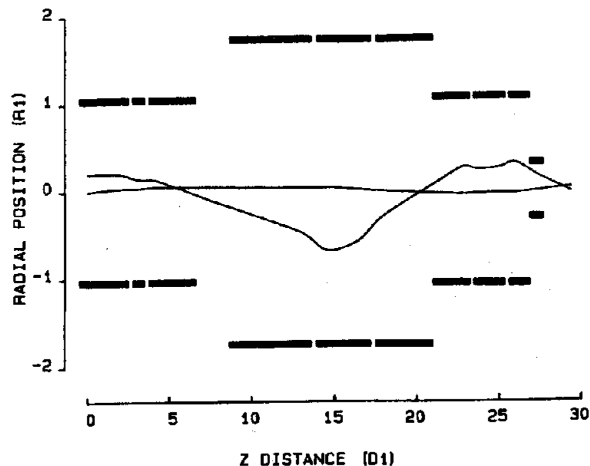

FIG. 7. Calculated ion trajectories through the three Einzel lenses added by the authors. Only the aperture at the end of lens 3 is shown and is elongated for modeling purposes. The rays start at the entrance of lens 1 and end at the sample position. The effect of space-charge divergence is not included. The voltage ratio for each lens is: lens 1; 3.1, lens 2; 0.24, lens 3; 4.5. The initial ($Z = 0$) and final ($Z = 29.5$) ray positions are given in Table II. The lens Z axis is marked in units of the diameter of lens 1 and the radial axis in units of the radius of lens 1.

TABLE II. The initial and calculated final ray positions for the ion beam path through the three lens system as determined by the program CHDEN. Space-charge forces were neglected. The applied lens voltages used for the calculation are listed. The initial position is at the entrance of lens 1. The final position is located at the sample and is given in units of the diameter of lens 1.

Initial and final ray positions:

	Initial ($Z = 0$)			Final ($Z = 29.5D_1$)		
Ray No.	Angle (°)	r/R_1	mm	Angle (°)	r/R_1	mm
1	0.0	0.20	1.5	−2.4	−0.015	−0.11
2	0.5	0.0	0.0	0.65	0.041	0.31

Lens voltages:
Lens 1: −1050 V
Lens 2: +380 V
Lens 3: −1750 V

Calculated beam diameter (mm): 0.84

3. Lens 3

This lens is also constructed using the new geometry described for lens 2. A 2-mm aperture is placed between lenses 2 and 3 to remove any particles from the beam which are out of focus. This allows the final spot diameter to be determined by the focusing characteristics of this final lens. The diameter of this lens was chosen to be as small as possible in order to avoid interference with the secondary ion angular spectra but yet to have a large enough diameter to provide adequate focusing. The use of the program CHDEN permitted us to choose a diameter which fulfilled both criteria. A 4-mm aperture is located at the end of the last element to isolate the lens from the fields in the raster plates. The last element of this lens is only $1.4D$ long in order to provide room for the raster plates. While this is long enough for the electric field to have disappeared, the exit aperture was found to influence the beam trajectory. Therefore, this aperture was included in the modeling of the lens. The beam must drift 38 mm to the target upon leaving lens 3.

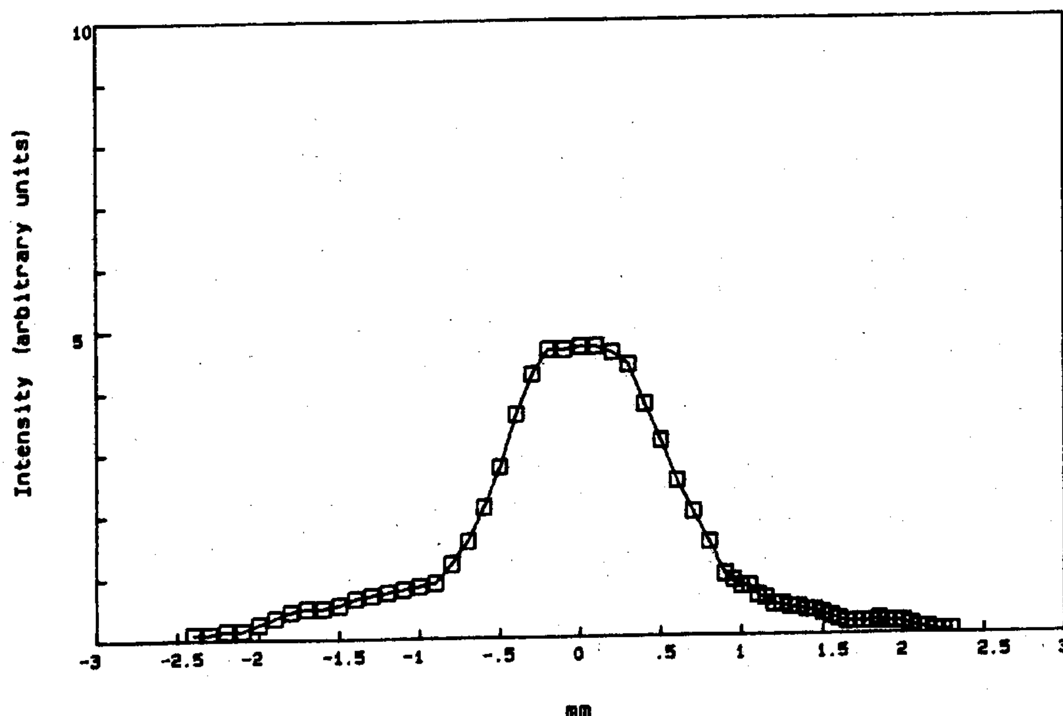

FIG. 8. The measured profile for a 0.72-μA, 500-eV beam of Ar^+ ions.

TABLE III. Predicted and actual lens voltages. The predicted values were determined by the program CHDEN neglecting space-charge forces.

Lens	Predicted voltage	Experimental voltage
1	− 1050	− 1035
2	+ 380	+ 480
3	− 1750	− 2980

E. Ion trajectories

Figure 7 displays the calculated beam trajectories for the complete lens assembly neglecting space-charge effects. The inclusion of space-charge divergence will be discussed in the next section. The beam is assumed to leave the velocity filter in a collimated fashion. The initial and final particle positions along with the predicted lens voltages are listed in Table II. As can be seen from the figure, the beam is well focused at the sample and is transported through the lens assembly without current loss at the various apertures.

III. RESULTS

The beam characteristics at the sample position are a current of 0.72 μA and a diameter of 1 mm for an Ar^+ beam at a potential of 500 eV. The current was measured using a stainless-steel plate attached to the sample holder. The ion current is believed to be a reasonably accurate measurement even though a Faraday cup was not used since the secondary electron emission is quite low at an incident kinetic energy of 500 eV.[22] The beam diameter was determined by three methods. The first measurement was performed by sputtering a phosphor film on the sample manipulator for several hours until the phosphor had been completely removed. The manipulator was then removed from the chamber and the sputtered hole in the phosphor measured with a ruler. The hole was measured to be 1.0 mm in diameter. Second, a 0.145-mm-diam tungsten wire was strung over an opening in the sample holder. The sputtered W^+ signal was measured as the sample holder was moved vertically with a vernier adjustment on the manipulator support. The measured beam profile is shown in Fig. 8. The profile is flat topped and has a FWHM of 1.19 mm. This profile is a convolution of the actual current distribution with a weighting function reflecting the differing length of wire covered by the ion beam at each measured point. The measured signal $S(x)$ is given by

$$S(x) = \int_x^{\infty} \frac{f(r)\,r\,dr}{\sqrt{r^2 - x^2}}, \qquad (7)$$

where $f(r)$ is the actual radial current distribution, r is the radial position from the center of the beam, and x is the radial position of the experimental data point. $f(r)$ was determined numerically by an Abel inversion of Eq. (7).[23] The corrected beam profile has a broader flat-top region and a FWHM of 1.12 mm. The third measurement was made by sputtering a crater in a silicon sample over a period of approximately 10 h. The crater profile was determined with a Talysurf profilometer. The crater profile appeared to be Gaussian and had a FWHM of 0.85 mm. The average beam diameter from these measurements is 0.99 ± 0.14 mm.

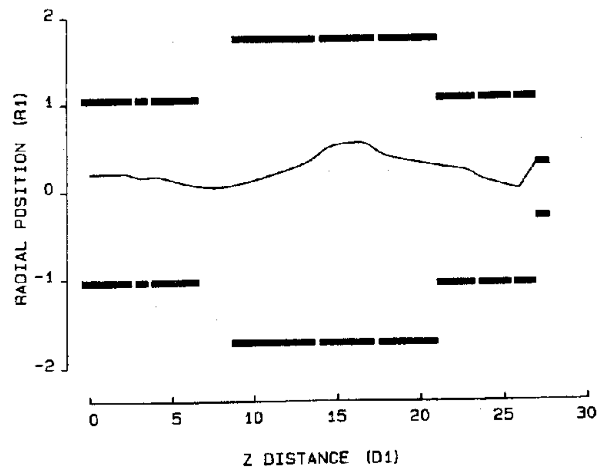

FIG. 9. The calculated ion beam path with space-charge forces included. The lens voltages are given in Table II.

The predicted lens voltages and the experimentally determined lens voltages are listed in Table III. With the exception of lens 1, the actual voltages are far different than the calculated voltages. This is due to the space-charge divergence present within the beam. Figure 9 shows the calculated beam path using the predicted voltages when the divergence due to space charge for a 500-eV beam of Ar^+ ions is included. The beam is poorly focused at the apertures between lenses 2 and 3 (not shown) and at the exit of lens 3. The rapid divergence of the beam near the end of lens 3 is due to strong coulombic repulsion as the beam gets very close to the lens axis. When the experimentally determined voltages are used in the trajectory calculation, the beam is much better focused (Fig. 10). In this case, the beam passes through the apertures and diverges as it drifts between lens 3 and the target. The beam diameter is calculated to be 3.0 mm. The qualitative agreement between the results of CHDEN and experiment is good.

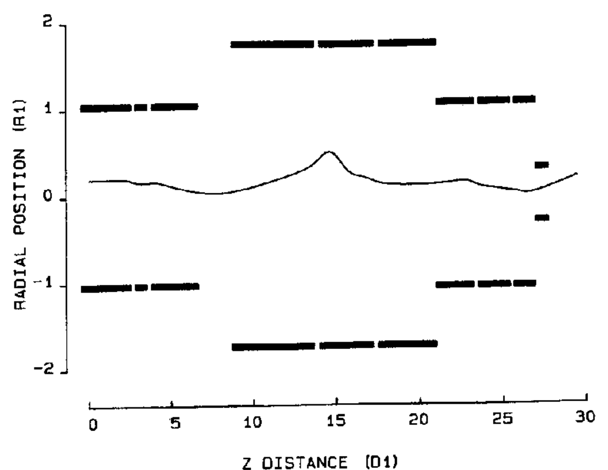

FIG. 10. The calculated ion beam path with space charge. The lens voltages used are the experimentally determined values listed in Table III. The voltage ratios are: lens 1; 3.07, lens 2; 0.04, lens 3; 6.96.

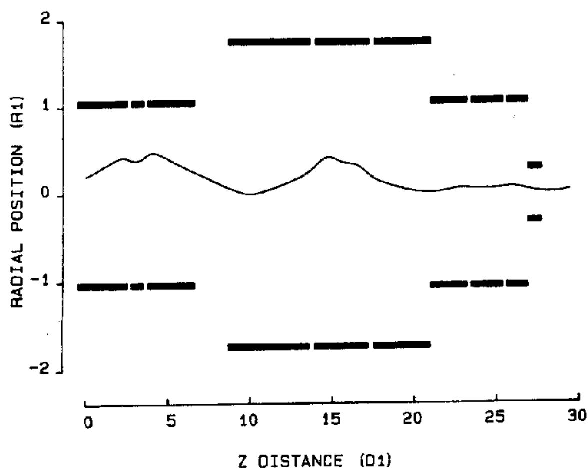

FIG. 11. The calculated ion beam path with space charge. The lens voltages are the experimentally determined values. The beam makes an angle of 3° to the lens axis at the entrance of lens 1.

Quantitatively, the program CHDEN predicts a much larger spot size than is observed. This discrepancy may be due to two of our initial assumptions. First, we assumed the beam would enter lens 1 in a collimated fashion. The beam may be spreading by space-charge forces or by the action of the extraction lens. In addition, the Wien filter is a focusing device and can introduce asymmetric beam aberrations.[14] Figure 11 shows the calculated beam path using the actual lens voltages with space-charge forces included, but in contrast to Fig. 10, the beam has an initial angle of 3° with respect to the lens axis. The calculated spot diameter is now 0.77 mm. It is likely that the beam has an initial angle as it enters lens 1. Second, we maintained a constant current of 0.72 μA throughout the beam path in the calculations by CHDEN. The beam may be partially neutralized by secondary electron emission from the electrodes or by gas phase charge exchange reactions. These effects would reduce the coulombic repulsive forces. The charge exchange reaction would be most pronounced prior to lens 2 due to the higher residual gas pressure in the ion gun. Also, the final spot size would be decreased by secondary electron emission from the target. This is not an important contribution since the electron yield is low ($\sim$0.1) (Ref. 22) and the electrons would interact with the beam over a short distance.

ACKNOWLEDGMENTS

We wish to thank the Office of Naval Research, the National Science Foundation, and the IBM Corporation for their support.

[1] K. E. Foley and N. Winograd, Surf. Sci. **122**, 541 (1982).
[2] P. H. Dawson and W. C. Tam, Surf. Sci. **91**, 153 (1980).
[3] P. H. Dawson, Surf. Sci. **65**, 41 (1977).
[4] R. J. Colton, SIMS V Springer Series in Chem. Phys. **44**, 456 (1986).
[5] R. G. Hart and C. B. Cooper, Surf. Sci. **94**, 105 (1980).
[6] W. Gerhard and H. Oechsner, Z. Phys. **B22**, 41 (1975).
[7] M. Hou and M. T. Robinson, Appl. Phys. **18**, 381 (1979).
[8] H. Oechsner, H. Paulus, and P. Beckman, J. Vac. Sci. Technol. A **3**, 1403 (1985).
[9] G. E. Thomas, L. J. Beckers, J. J. Vrakking, and B. R. deKonig, J. Cryst. Growth **56**, 557 (1982).
[10] R. A. Gibbs and N. Winograd, Rev. Sci. Instrum. **52**, 1148 (1981).
[11] H. Liebl, J. Bohdansky, J. Roth, and V. Dose, Rev. Sci. Instrum. **58**, 1830 (1987).
[12] J. Kirschner, Rev. Sci. Instrum. **57**, 2640 (1986).
[13] P. Kirstein, G. Kino, and W. E. Waters, *Space Charge Flow* (McGraw-Hill, New York, 1967).
[14] R. G. Wilson and G. R. Brewer, *Ion Beams With Applications to Ion Implantation* (Wiley, New York, 1973).
[15] H. S. W. Massey, E. H. S. Burhop, and H. B. Gilbody, *Electronic and Ionic Impact Phonomena, Vol IV* (Oxford University, Oxford, 1974).
[16] E. Harting and F. H. Read, *Electrostatic Lenses* (Elsevier Scientific, New York, 1976).
[17] I. W. Drummond, Vacuum **34**, 51 (1984).
[18] The program is available in an operational form appropriate for an IBM AT or compatible from Focussed Software, 871 Southgate Drive, State College, PA 16801.
[19] A. Renau, F. H. Read, and J. N. H. Brunt, J. Phys. E **15**, 347 (1982).
[20] Ion Gun model G-2 (Colutron Corp, Boulder, CO).
[21] A. Septier, in *Focusing of Charged Particles*, edited by A. Septier (Academic, New York, 1967).
[22] R. A. Baragiola, E. V. Alonso, J. Ferron, and A. Olivia-Florio, Surf. Sci. **90**, 240 (1979).
[23] I. J. D. Craig and J. C. Brown, *Inverse Problems in Astronomy* (Hilger, Bristol, England, 1986).